




# Single-step femtosecond laser-induced formation of coexisting microstructures in silicon

LUIS HUMBERTO ROBLEDO-TABOADA<sup>1</sup>, JAVIER FRANCISCO JIMÉNEZ-JARQUÍN<sup>1</sup>,  
MARIELA FLORES-CASTAÑEDA<sup>2,5</sup>, ANTONIO MÉNDEZ-BLAS<sup>3</sup>, JACOB  
BARRANCO-CISNEROS<sup>4</sup> and SANTIAGO CAMACHO-LÓPEZ<sup>2,\*</sup> 

<sup>1</sup>Oaxaca Institute of Technology/Mexico National Institute of Technology, C.P. 68030 Oaxaca, Mexico

<sup>2</sup>Optics Department, Center for Scientific Research and Higher Education of Ensenada, C.P. 22860 Ensenada, Mexico

<sup>3</sup>Physics Institute, Benemerita Autonomous University of Puebla, C.P. 72570 Puebla, Mexico

<sup>4</sup>Institute of Optical Communications Research, Autonomous University of San Luis Potosí, C.P. 78210 San Luis Potosí, Mexico

<sup>5</sup>Researchers for Mexico CONACyT, Center for Scientific Research and Higher Education of Ensenada, C.P. 22860 Ensenada, Mexico

\*Author for correspondence (camachol@cicese.mx)

MS received 31 May 2022; accepted 23 December 2022

**Abstract.** Various micron and submicron structures were laser-induced on silicon, including LIPSS (laser-induced periodic surface structures), grooves, conical spikes and deep craters. We used a fibre-based femtosecond (fs) laser to ablate the silicon wafer in ambient air. The formed structures strongly depend on the per-pulse laser fluence and the number of delivered pulses. We characterized the obtained structures using electron scanning microscopy and atomic force microscopy. Our results revealed interesting features such as flipping structure orientation and the coexistence of two or more types of structures that exhibit a unique wetting behaviour (contact angle with water). We found that the type of surface structures significantly influences the surface wettability.

**Keywords.** Silicon microstructures; fibre-based femtosecond laser pulses; laser ablation.

## 1. Introduction

There are many different methods dedicated to surface texturing of a variety of materials, methods such as laser ablation [1–5], electrochemistry [6–8], chemical etching [9, 10], sputtering [11], plasma [12] and photochemistry [13] can be readily found in the literature. The importance of these methods lies not only in the precision and control of the texturing but also in the envisioned applications of the textured materials obtained through these techniques. Surfaces with functional properties such as hydrophilicity [14, 15] and hydrophobicity [3, 8, 16, 17] are made possible through texturing; also, surface texturing can tune the material's optical properties [2], and even the tribological features of a given material can be modified on demand through surface texturing [8].

The micro and nanostructuring of silicon through ultra-short pulse lasers has been widely studied in recent years [18–22], showing applications that include optoelectronic devices, microfluidics, biomedicine and superhydrophobic devices [19].

It is well known that the presence of oxygen during the ablation process in silicon can influence the process itself and also the structural and chemical composition characteristics of silicon at its surface. Most of the current reports on femtosecond laser microstructured silicon are carried out either under a gas environment [22, 23] or vacuum [24, 25]. Recent research reports have shown the formation of conical structures in silicon doped with chalcogenide species (sulphur, selenium and tellurium) [26–29]. We must note that the cone formation in silicon using laser ablation has been reported in the literature mainly for processing with titanium-sapphire (fs, 800 nm), Nd: YAG (ns, 1064 nm) and excimer (ns, 248 nm) pulsed lasers. However, to date, there have been no reports of the direct fabrication of conical microstructures in silicon using Yb-doped fibre lasers at a wavelength of 1030 nm and a pulse duration of 270 fs.

In this work, we report on the formation and characterization of various micro and submicron structures obtained through femtosecond laser ablation of silicon in ambient air and the wetting properties of the laser-structured silicon surface.

## 2. Experimental

For all the experiments, we used a high resistivity (5–10  $\Omega$  cm) silicon wafer, boron p-doped type, Si (100) cut to a size of 1 cm<sup>2</sup>. The processing laser used in these experiments was a Satsuma HP2 model from Amplitude Systèmes. It delivers a TEM<sub>00</sub> Gaussian intensity profile laser beam ( $M^2 = 1.1$ ). The laser pulse duration was 270 fs with an emission wavelength centred at 1030 nm. We used the experimental setup depicted in figure 1.

The process of formation of distinct structures by the laser ablation technique used an aspherical converging lens of 25 mm focal distance, which produces a beam waist diameter of 14  $\mu$ m (FW1/e<sup>2</sup>M) at  $z = 0$ ; the experiments were carried out in ambient air at atmospheric pressure. We ablated the silicon sample with the wafer surface at three different positions with respect to the laser beam waist (see figure 2). The beam waist at the surface ( $z = 0$ ) and then the sample is displaced downwards ( $z = d_1$  and  $z = d_2$ ) such that the beam waist lies above the surface. This permitted to vary the delivered ablation fluence (by changing the laser beam cross-section area on the surface of the sample), which allowed to obtain three different types of morphological structures: craters, conical spikes and LIPSS (laser-induced periodic surface structures). Each of the reported microstructures

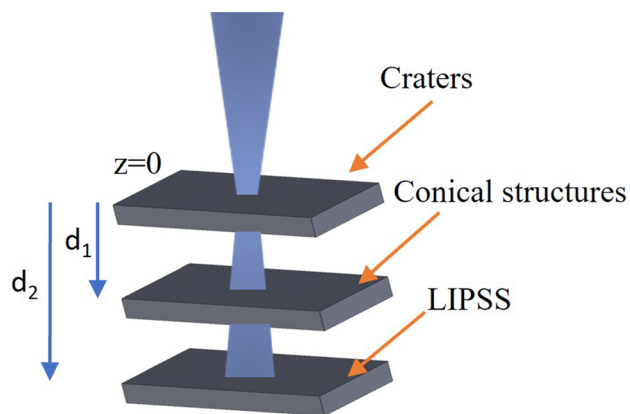


**Figure 2.** Varying the delivered laser fluence, while keeping the energy per pulse constant, is achieved by positioning the sample surface at different distances from the beam waist.

were obtained under different fluences per pulse; craters were obtained at a fluence of 753 mJ cm<sup>-2</sup>, conical peaks form at a fluence of 651 mJ cm<sup>-2</sup>, while the LIPSS formation requires a fluence of 596 mJ cm<sup>-2</sup>. The laser fluence is defined as  $F_p = \frac{E_p}{A_{\text{eff}}}$ , where  $F_p$  is the fluence per pulse,  $E_p$  the energy per pulse and  $A_{\text{eff}}$  is the effective cross-section area of the incident laser beam at the silicon sample surface.

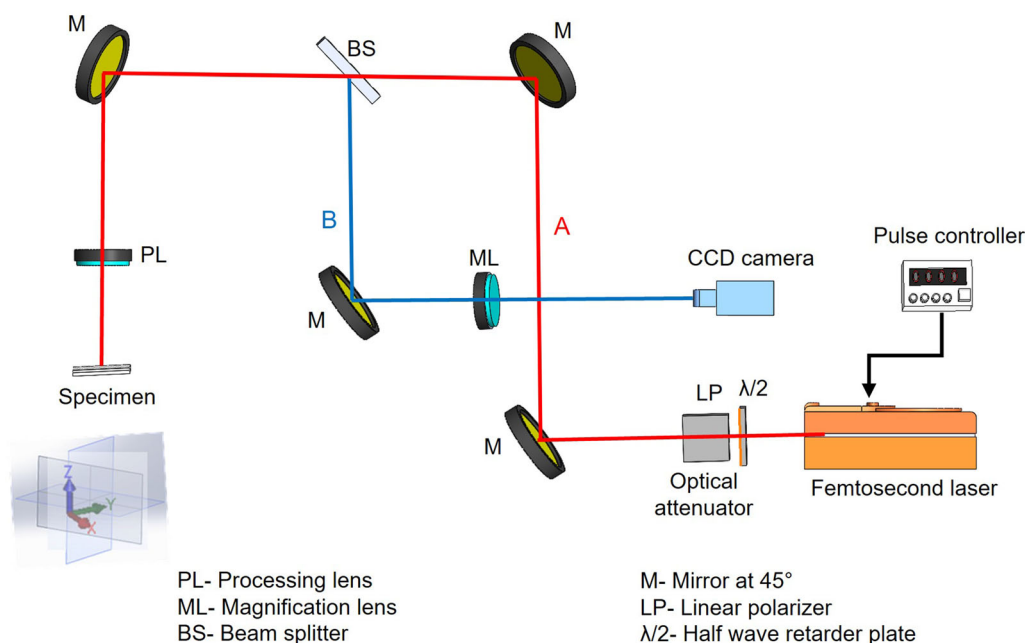


**Figure 1.** Experimental set up. The laser pulses are conducted through a series of mirrors down to the silicon wafer (optical path A in red). An optical attenuator allows the adjusting of the energy per pulse. An image relay system (optical path B in blue) is used to image the laser beam waist at the surface of the wafer onto a CCD camera. In addition, the experimental arrangement is complemented with an X-Y-Z translation stage to displace the sample with respect to the laser beam and a pair of goniometers to adjust the angle of incidence.

### 3. Results and discussion

#### 3.1 Formation of three distinct structures for varying laser fluence

Figure 3 shows SEM micrographs of the three different synthesized microstructures. It is important to highlight the distinct features of the formed structures according to the per-pulse laser fluence. LIPSS are obtained with a relatively

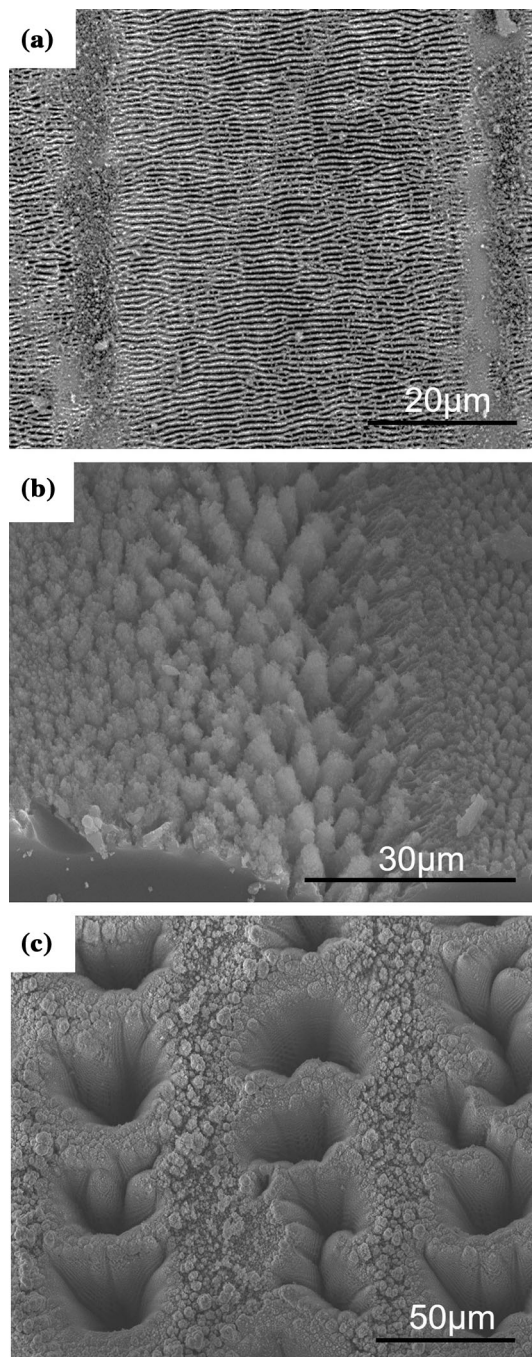


**Figure 3.** SEM micrographs of silicon structures produced through laser ablation: (a) LIPSS, (b) conical structures and (c) deep craters.

low laser fluence of  $596 \text{ mJ cm}^{-2}$  (figure 3a); by increasing the laser fluence up to  $651 \text{ mJ cm}^{-2}$ , we obtain conical spikes (figure 3b); further increasing the laser fluence up to  $753 \text{ mJ cm}^{-2}$  produces deep craters (figure 3c).

The conical structures obtained in our case under ambient air conditions are similar to the ones reported by Wu *et al* [30], both structures are produced in air environment at atmospheric pressure and show superficial dendritic structures with size on the order of 10 to 100 nm, however, our cones differ in height (6 vs.  $24.4 \mu\text{m}$ ) and width ( $5.3$  vs.  $11 \mu\text{m}$ ) when compared against Wu's cones (see table 1).

When contrasted against conical structures processed under other environments, we found that our structures grow differently in size, profile (sharp structures) and periodicity as compared to those reported for laser ablation in  $\text{SF}_6$  environment [23, 31] or in the presence of a chalcogenide coating [26, 29] (see table 1). In general, our cones are shorter and narrower.

#### 3.2 Structure formation as a function of the number of pulses

The silicon substrate was mounted on a computer-controlled  $x$ - $y$ - $z$  translation stage to conveniently reposition the sample at different irradiation spots. Six sites were irradiated on the silicon substrate with 50, 300, 400, 500, 700 and 900 pulses each (see figure 4) at 1 kHz repetition rate and a fluence per pulse of  $651 \text{ mJ cm}^{-2}$ .

Once the optimal per-pulse laser fluence for the formation of conical structures was determined, experiments were carried out to explore the evolution of various structures formation as a function of the number of pulses. Figure 5 shows the formation of three types of coexisting structures ranging from periodic ones (LIPSS) at 50 pulses, grooves and conical structures at 400 pulses and deep craters at 900 pulses.

A close-up view of the laser irradiated spots in figure 5 clearly shows LIPSS formation at the outer edge of the ablated crater, while spikes consolidate right in the centre of the crater (figure 5a), notice also a transition area with what seems to be molten filaments partially covering the LIPSS area. Grooves always form between the spikes and the LIPSS regions (figure 5b). When the craters are fully formed and as a consequence, the outer LIPSS, grooves and spikes have been ablated off, noticeably the crater walls are fully covered by LIPSS with a near  $+45^\circ$  and  $-45^\circ$  orientation with respect to the crater longitudinal axis (figure 5c).

For the range of pulses used in the experiments (ranging from 50 to 2000), the periodicity of the LIPSS and groove structures are summarized in table 2. It is in the order of half the wavelength for LIPSS, with an exception for the 2000 pulses case for which the LIPSS periodicity grows larger than a full wavelength; and it is three times the wavelength for grooves.

**Table 1.** Summary of synthesis and properties of femtosecond laser ablated silicon.

Laser	Environment or coating	Fluence	Pulses	Periodicity ( $\mu\text{m}$ )	Speck morphology	Height and width ( $\mu\text{m}$ )
Yb: KGW	SF <sub>6</sub>	0.38 J cm <sup>-2</sup>	200	4.1	Tall and sharp structures	8 and 2.5
$\lambda = 1026$ nm and 170 fs [31]						
Ti: Al <sub>2</sub> O <sub>3</sub>	SF <sub>6</sub>	10 kJ m <sup>-2</sup>	600	4.3	Wide and sharp structures	10 and 5
$\lambda = 800$ nm and 100 fs [23]						
Ti: Al <sub>2</sub> O <sub>3</sub>	Tellurium	0.85 J cm <sup>-2</sup>	—	3.5	Coarse structures with superficial dendritic structures	11 and 6
$\lambda = 800$ nm and 50 fs [26]						
Ti: Al <sub>2</sub> O <sub>3</sub>	Sulphur powder	10 kJ m <sup>-2</sup>	—	9.5	Wide, blunt structures	12 and 11
$\lambda = 800$ nm and 100 fs [29]						
Ti: Al <sub>2</sub> O <sub>3</sub>	Selenium powder	10 kJ m <sup>-2</sup>	—	10.1	Wide, blunt structures	12 and 13
$\lambda = 800$ nm and 100 fs [29]						
Ti: Al <sub>2</sub> O <sub>3</sub>	Air	33 kJ m <sup>-2</sup>	—	12.5	Coarse structures with superficial dendritic structures	24.4 and 11
$\lambda = 800$ nm and 100 fs [30]						
Yb -doped fibre	Air	651 mJ cm <sup>-2</sup>	400	7	Coarse structures with superficial dendritic structures	6 and 5.3
$\lambda = 1030$ nm and 270 fs						

[present work]

Our LIPSS and grooves show periodicity which agrees well with those reported by Tsibidis *et al* [19]. They also report the coexistence of three types of structures (LIPSS, grooves and spikes). Although in their case, the formation of LIPSS occurs with an orientation perpendicular to the polarization, while in our case as shown in figure 3a LIPSS are formed parallel to the incident beam polarization. As per their grooves those form parallel to polarization [19], while our grooves are always perpendicular to the incident beam polarization, as seen in figure 3b.

The formation of LIPSS inside the crater is attributed to the interference of incident light with scattered light within the crater (notice the periodicity close to  $\lambda/2$ ), because of the oblique incidence on the crater wall due to the diverging beam passing the beam waist, as well as polarization. It is worth mentioning that various groups have previously reported the formation of rings in silicon (attributed to shock waves) [32], periodic structures in the crater (due to radiation dose and laser polarization) [33], and craters with superficial defects (a consequence of fluence and number of pulses) [34].

### 3.3 Production of large textured areas

Regarding the manufacture of structures in large areas, once both the optimal per-pulse laser fluence and the number of pulses were set for the formation of conical spike structures, large structured samples (1 cm<sup>2</sup>) were manufactured. This was achieved by combining the process of laser ablation and sample computer-controlled displacement in the X and Y axes. Linear sweeps of 10,000  $\mu\text{m}$  in the X direction were performed, each time a sweep was completed the laser was shut with a programmed gate, then a 70  $\mu\text{m}$  perpendicular displacement was carried out in the Y direction to give way to a new sweep. This was repeated steadily until a large, homogeneous laser processed area was completed. All samples were laser processed with a scan speed of 250  $\mu\text{m s}^{-1}$ , a pulse repetition rate of 1 kHz, and a per pulse laser fluence of 651 mJ cm<sup>-2</sup>.

Figure 6 shows an optical image of a representative 1 cm<sup>2</sup> laser-processed silicon sample (figure 6a) and atomic force microscopy micrographs of typical silicon surfaces treated under the appropriate laser irradiation conditions for the formation of LIPSS, spikes and a channel (figure 6b).

Scanning electron microscopy (SEM) micrographs of the large area processed surface are shown in figure 7. The overall landscape is seen in figure 7a, it can be observed that large-size spikes dominate in the area corresponding to the maximum intensity of the Gaussian laser beam profile, i.e., the hottest region during the laser scan. The spike size decreases towards the edges of the laser scanned area to finally give way to the formation of LIPSS (figure 7b). A close-up of a transversal cut profile (figure 7c) reveals the typical size of a conical spike structure, which is in the order of 6.04  $\mu\text{m}$  tall and 5.28  $\mu\text{m}$  width at its base.

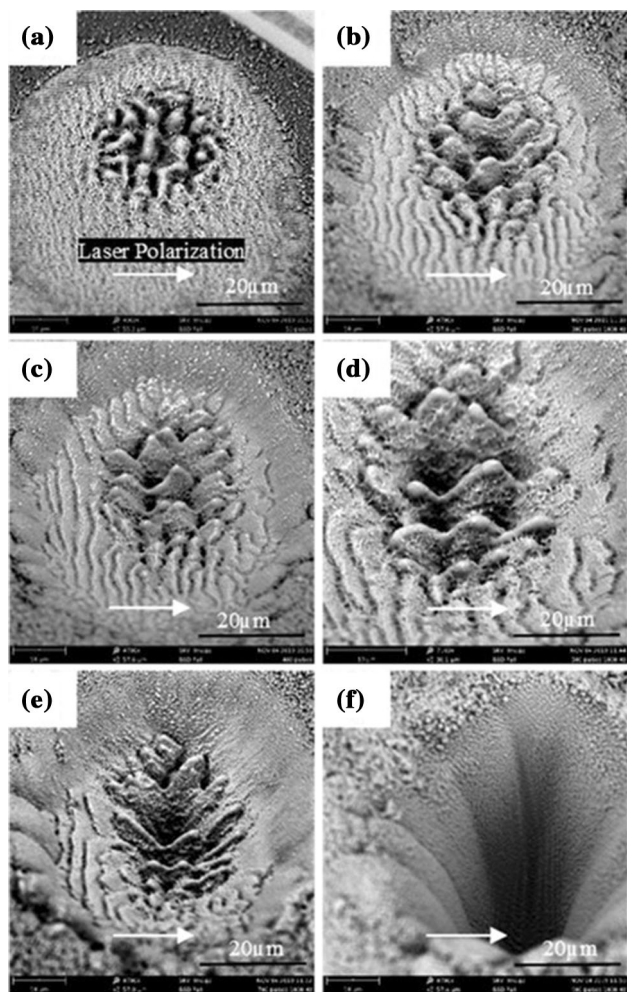


**Figure 4.** Growth of coexisting structures under laser processing at a varying number of pulses: (a) 50, (b) 300, (c) 400, (d) 500, (e) 700 and (f) 900 pulses.

### 3.4 Surface wettability

Contact-angle analysis was performed to examine the wettability of the laser-processed silicon wafers. Hydric behaviour was determined via contact-angle analysis using the water drop method. A 10 μl volume was dropped on the structured surface and images of the drop were captured with the help of a high-definition camera (Canon XA25). We used the Image J open software for image processing. The crystalline silicon wafer showed a contact angle of 39° (figure 8a). The wafer with LIPSS showed similar behaviour to the unirradiated silicon with a smaller contact 36° angle (figure 8b). The surface with the conical spikes produced a hydrophilic behaviour showing a 7° contact angle (figure 8c). The hydrophilicity is further enhanced by the surface with craters with a superhydrophilic behaviour and a contact angle of just 4° (figure 8d). It is clear that the surface wettability is affected by the type of surface structure, in the case of LIPSS these are too shallow structures as to generate a capillarity effect, on the contrary both the spikes and craters are depth

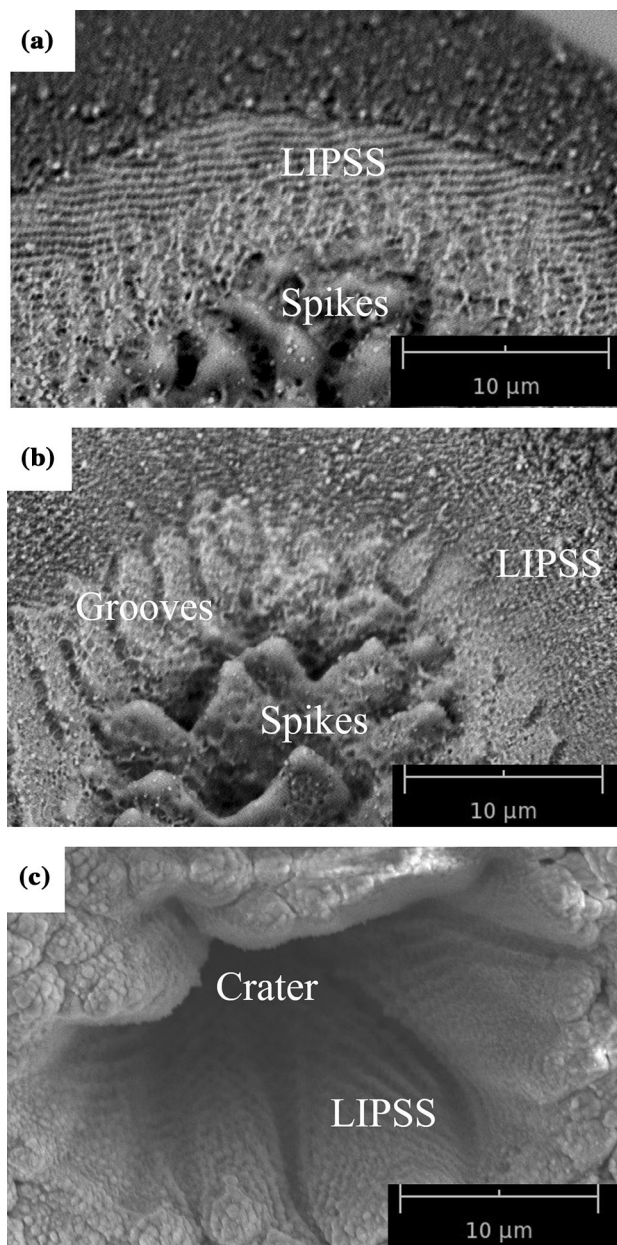


**Figure 5.** Close-up view of the different structures that form under different number of pulses: (a) 50, (b) 400 and (c) 900.

structures because they are created under delivered laser fluences above the ablation threshold. This allows for the capillarity effect to become dominant, therefore setting a hydrophilic behaviour of the surface, i.e., low contact angles.

Our samples produced in large areas (1 cm<sup>2</sup>) have hydrophilic behaviour ( $\theta < 90$ ). The samples made with high energy density (753 mJ cm<sup>-2</sup>) are similar to those reported in Vorobyev *et al* [14, 15] study, these are composed of deep (39.6 μm) and wide (42.6 μm) craters with surface dendritic structures and a high wettability or superhydrophilic behaviour. Interestingly, the samples with conical spikes show a wetting behaviour that differs from the one reported by Baldacchini *et al* [16] and Zorba *et al*

**Table 2.** Periodicity of the LIPSS and grooves as a function of the number of pulses, measured directly from the SEM micrographs.

Pulses	Periodicity (nm)	
	LIPSS	Grooves
50	633	None
300	525	2655
400	547	3424
500	542	3191
600	571	2987
700	511	3155
900	551	None
2000	1295	None

[17], where the surface is hydrophobic ( $\theta > 90$ ). This can be explained by the microstructure dimensions (height  $> 22.5$   $\mu\text{m}$ , width  $< 5$   $\mu\text{m}$  and space between cones  $< 3$   $\mu\text{m}$ ) and the processing SF6 environment. Our conical structures have a smaller size (height = 6.04  $\mu\text{m}$ , width = 5.28  $\mu\text{m}$ ) and a larger cone-to-cone spacing of 7  $\mu\text{m}$ . In the case of LIPSS, the wetting features are similar to crystalline silicon.

The results presented in this work show that we have a versatile method for tailoring the wettability of a silicon surface. This by conveniently adjusting either the per-pulse laser fluence or the number of pulses delivered during the ablation process, since these two parameters set the conditions for obtaining the surface structure type of interest.

This is a rapid single-step texturing process that offers advantages over other methods, such as chemical etching or multi-step lithography, that can produce similar surface texturing.

#### 4. Conclusions

It was demonstrated that three types of micro and submicron structures (LIPSS, grooves and conical spikes) can be created at once on crystalline silicon by using femtosecond laser pulses. At high enough laser fluence, these structures are ablated off to form deep craters whose walls are textured by LIPSS. The conical spikes, grooves and LIPSS are clearly dependent on the local laser fluence across the laser beam. The orientation of the LIPSS is parallel to the incident laser beam polarization, and on the contrary, the grooves are oriented perpendicular to the polarization. An interesting finding is that as the number of pulses increases, the grooves initially formed at the centre of the irradiated spot, flip their orientation from perpendicular to parallel to the incident laser beam polarization. On a challenging task, it was possible to find adequate laser irradiation parameters to process a large area on the silicon wafer, so that it was filled with conical spikes, grooves, LIPSS and craters. This led to the modification of the silicon surface wettability going from a  $39^\circ$  contact angle for the pristine crystalline silicon wafer to a superhydrophilic surface at  $4^\circ$  when craters dominate over the other type of surface structures.

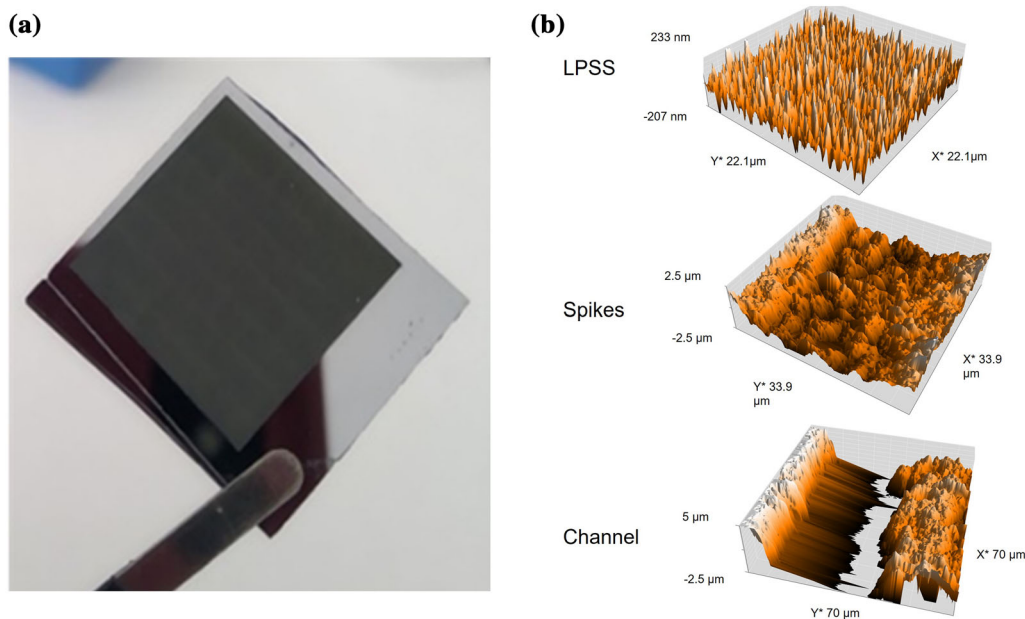


**Figure 6.** (a) Laser-processed silicon sample and (b) atomic force microscopy micrographs of typical LIPSS, conical spikes and a channel within the laser-processed silicon surfaces.

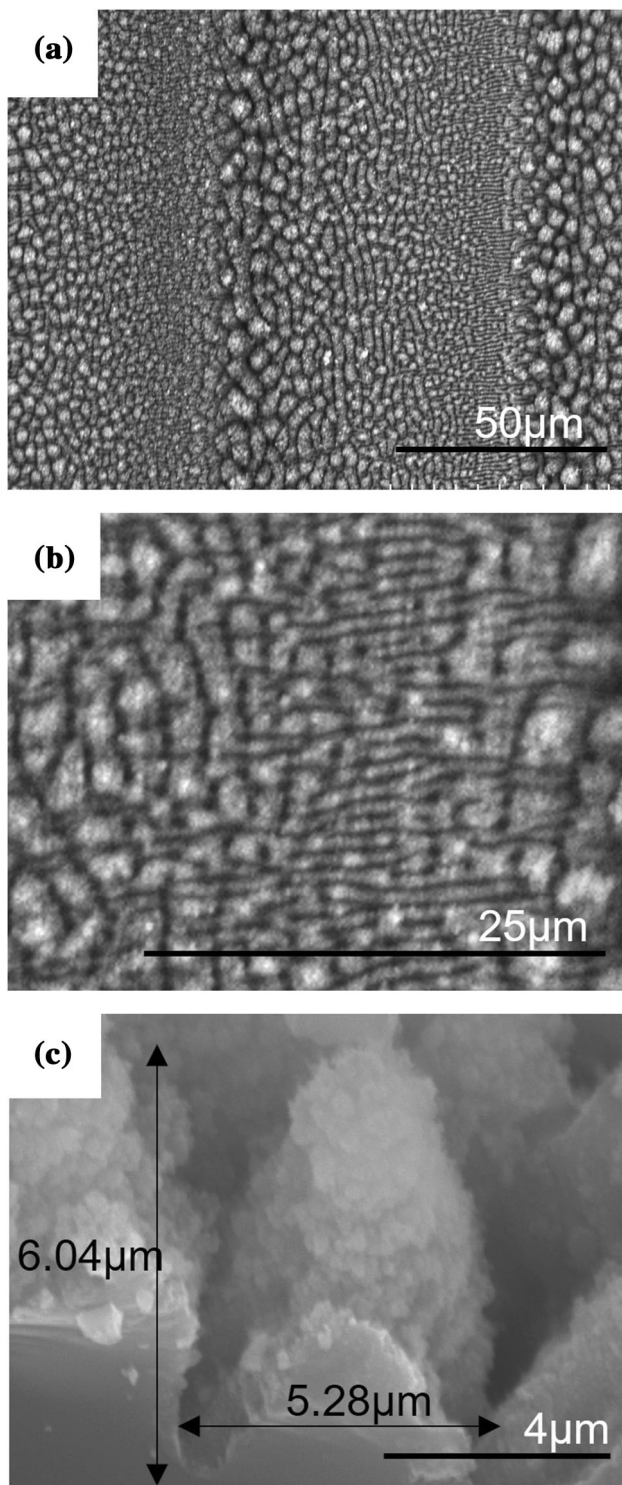


**Figure 7.** (a) Laser-processed silicon surface showing conical spikes and LIPSS. (b) Magnification of panel a, notice that the LIPSS are formed parallel to the direction of the incident laser polarization, and its periodicity is of 682 nm. (c) View of the conical structures at a 90° cross-section cut, notice that although the surface of the cone shows granular morphology, its core is fully solid.

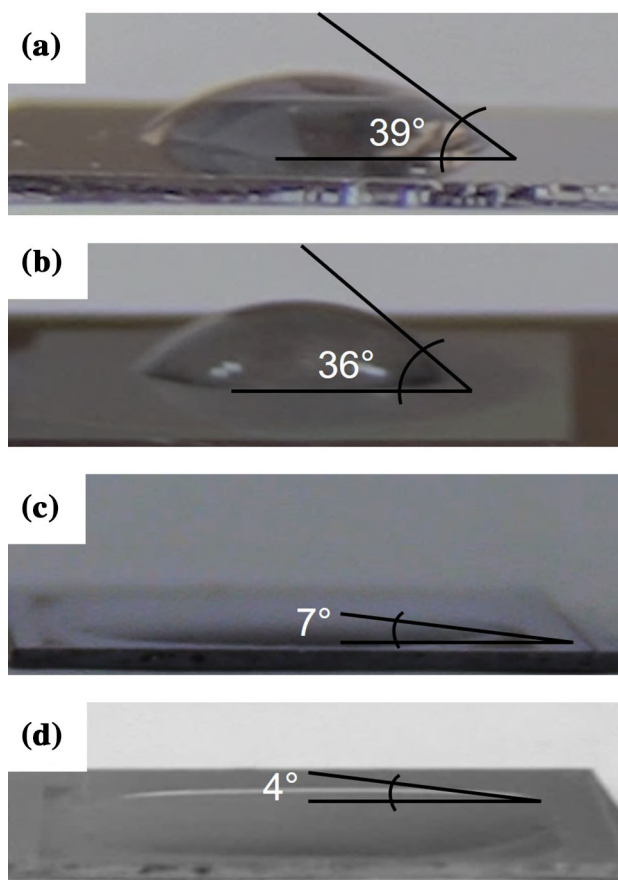


**Figure 8.** Liquid–solid contact angle for different silicon laser-textured surfaces. (a) The crystalline silicon wafer, (b) the silicon surface with LIPSS, (c) the silicon surface with conical spikes and (d) the silicon surface with craters.

**Acknowledgements**

Luis Humberto Robledo-Taboada acknowledges the National Council of Science and Technology (CONACyT) for the scholarship for postgraduate studies (791059). Santiago Camacho-Lopez acknowledges CONACyT partial support to the present work through grant FORDECyT-PRONACES 246648.

**References**

- [1] Linde D V L, Tinten K S and Bialkowski J 1997 *Appl. Surf. Sci.* **109** 1
- [2] Carey J E, Crouch C H and Mazur E 2003 *Opt. Photonics News* **1047** 32
- [3] Halbwax M, Sarnet T, Delaporte P, Sentis M, Etienne H, Torregrosa F *et al* 2008 *Thin Solid Films* **516** 6791
- [4] Chen T, Si J, Hou X, Kanehira S, Miura K and Hirao K 2011 *J. Appl. Phys.* **110** 1
- [5] Vorobyev A Y and Guo C 2011 *Appl. Surf. Sci.* **257** 7291

- [6] Sailor M J 2012 (ed) *Porous silicon in practice preparation characterization and applications* (Wiley-VCH USA) p 6
- [7] Canham LT 1997 (ed) *Engineers properties of porous silicon* (London: Inspec, The Institution of Electrical Engineers) p 12
- [8] Liu Y H, Wang X K, Luo J B and Lu X C 2009 *Appl. Surf. Sci.* **255** 9430
- [9] Huang Z, Geyer N, Werner P, Boor J and Gösele U 2011 *Adv. Mater.* **23** 285
- [10] Venkatesan R, Arivalagan M K, Venkatachalapathy V, Pearce J M and Mayandi J 2018 *Mater. Lett.* **221** 206
- [11] Srodsky M H, Cardona M and Cuomo J J 1977 *Phys. Rev. B* **16** 3556
- [12] Ruby D S, Zaidi S H, Narayanan S, Damiani B M and Rohatgi A 2002 *Sol. Energy Mater. Sol. Cells* **74** 133
- [13] Kolasinski K W 2018 in *Silicon surface photochemistry*, Vol. 2, K Wandelt (ed) (Elsevier, Oxford) p 611–620. <https://doi.org/10.1016/B978-0-12-409547-2.14046-6>
- [14] Vorobyev A Y, Guo C, Gravesen P and Branebjerg J 2010 *Opt. Express* **18** 6455
- [15] Vorobyev A Y and Guo C 2013 *Laser Photonics Rev.* **7** 385
- [16] Baldacchini T, Carey J E, Zhou M and Mazur E 2006 *Langmuir* **22** 4917
- [17] Zorba V, Persano L, Pisignano D, Athanassiou A, Stratakis E, Cingolani R *et al* 2006 *Nanotechnology* **17** 3234
- [18] Her T H, Finlay R J, Wu C, Deliwala S and Mazur E 1998 *Appl. Phys. Lett.* **73** 1673
- [19] Tsibidis G D, Fotakis C and Stratakis E 2015 *Phys. Rev. B Condens. Matter Mater. Phys.* **92** 041405–041411
- [20] Sundaram S K and Mazur E 2002 *Nat. Mater.* **1** 217
- [21] Stratakis E 2012 *Sci. Adv. Mater.* **4** 407
- [22] Sun H, Liu X, Zhao L, Jia J, Jiang C, Xiao J *et al* 2022 *Opt. Express* **30** 1808
- [23] Sheehy M A, Winston L, Carey J E, Friend C M and Mazur E 2005 *Chem. Mater.* **17** 3582
- [24] Besner S, Degorce J Y, Kabashin A and Meunier M 2005 *Appl. Surf. Sci.* **247** 163
- [25] Li C H, Zhao J H, Chen Q D, Feng J, Zheng W T and Sun H B 2015 *IEEE Photonics Technol. Lett.* **27** 1481
- [26] Ma Y, Ren H, Si J, Sun X, Shi H, Chen T *et al* 2012 *Appl. Surf. Sci.* **261** 722
- [27] Su Y, Yao D, Wang S, Zhan X P and Xu H 2020 *Opt. Laser Technol.* **123** 1
- [28] Shi Y, Wu Z, Du L, Li S and Jiang Y 2018 *J. Mater. Sci.: Mater. Electron.* **29** 4526
- [29] Sheehy M A, Tull B R, Friend C M and Mazur E 2007 *Mater. Sci. Eng. B Solid-State Mater. Adv. Technol.* **137** 289
- [30] Wu C, Crouch C H, Zhao L and Mazur E 2002 *Appl. Phys. Lett.* **81** 1999
- [31] Skoulas E, Tsibidis G D and Stratakis E 2020 *J. Optoelectron. Adv. Mater.* **1** 501
- [32] Panchatsharam S, Tan B and Venkatakrishnan K 2009 *J. Appl. Phys.* **105** 093103–093111
- [33] Varlamova O and Reif J 2013 *J. Laser Micro Nanoeng.* **8** 300
- [34] Bonse J, Baudach S, Krüger J, Kautek W and Lenzner M 2002 *Appl. Phys. A: Mater. Sci. Process.* **74** 19